2

Modelling Hard Electron Energy Spectrum

2.1 Introduction

The non-thermal electron distribution, which produces the afterglow synchrotron radiation, is assumed to be distributed as a power law in energy, of the form given by equation 1.11. The standard fireball model assumes the power law index p of the distribution to be greater than 2, leading to simplification of theoretical models. Accommodating harder electron energy spectra, with values of $p < 2$, requires modifications in some of the basic expressions of the model because the upper cutoff of the distribution can not be neglected.

2.2 Modified Electron Distribution and the Injection Break

The upper cut-off γ_u of equation 1.11, depends on the micro-physics in the shock downstream. Nature of the distribution beyond this upper cutoff could be a sharp drop or a steeper ($p > 2$) powerlaw. Bhattacharya 2001 [15, hereafter B01] has used a γ_u which is a function of the bulk lorentz factor (Γ) of the shock. The

dependence on Γ is parametrised by an index q.

$$\gamma_u = \xi \Gamma^q \tag{2.1}$$

The time dependence of γ_m is altered by the introduction of γ_u. This in turn modifies the spectral evolution. Moreover, a new break frequency corresponding to γ_u will appear in the spectrum.

Dai & Cheng 2001 [35, hereafter DC01] has followed the same approach but with a special case of γ_u (their notation is γ_M) where $\gamma_M m_e c^2$ is the energy in which acceleration time scale for the particle exceeds its cooling time scale. Their model is a special case of B01 with $q = -1/2$. But this upper limit γ_M, in typical conditions lie at very high energies, so any observable feature of a corresponding break ν_M is unlikely to be seen.

Panaitescu & Kumar 2001 [98, hereafter PK01] consider two conditions to determine the upper limit of the hard electron energy distribution. (i) The upper limit (γ_{M1}) results when the acceleration mechanism is overtaken by the radiative energy loss, and the corresponding break frequency lies much above the observation limit. (ii) In the second case, the upper cut-off (γ_{M2}) is determined by the amount of energy available to electrons. A steeper powerlaw is assumed beyond the cutoff. Nature and temporal evolution of γ_{M2} is not considered, as a result, evolution of other breaks and the spectrum remains the same as that of the standard model. In reality, γ_{M2} is a result of some process which terminates the acceleration process and its time evolution is important in determining the spectral evolution of the afterglow. One cannot expect the same lightcurve decay indices as the standard model.

In this chapter, we continue the investigation of B01. The upper cutoff γ_u of B01 (equation 2.1) is identified as an injection break γ_i. We assume a steeper powerlaw beyond this lorentz factor. The major difference we have, from the previous works is q-dependent lightcurve evolution. We present analytical estimates for the lightcurve slope in terms of q.

2.3 Equations of Dynamics : Modifications by Huang et al.

We consider the fireball evolution from ultra-relativistic to newtonian regime. The equations used in defining the dynamics of the ultra-relativistic shock are given in chapter 1 (equations 1.6 to 1.8).

From equation 1.8, M at any distance r can be written in terms of m as,
$\int_{M_{\rm ej}}^{M} dM = \int_0^m [(1-\epsilon)\Gamma + \epsilon]\, dm$
Hence, $M = M_{\rm ej} + [(1-\epsilon)\Gamma + \epsilon]\, m$

In the adiabatic condition (which we will be concerned about, in this chapter), the thermal energy radiated away is negligible, or in other words $\epsilon = 0$. This will reduce equation 1.7 to

$$\frac{d\Gamma}{dm} = -\frac{\Gamma^2 - 1}{\Gamma m + M_{\rm ej}} \tag{2.2}$$

dm, is the amount of mass swept up by the shock at a distance r from the ambient medium of density $\rho(r)$, which is given by equation 1.9 Equation 1.6, defining the time elapsed in the observer's frame, after the redshift correction will become,

$$dt = \frac{dr}{2(1+z)\Gamma^2 c} \tag{2.3}$$

Only in rare cases the non-relativistic transition has been observed so far [50, 111] and it was treated separately from the ultra-relativistic phase since the expressions used dealt only with the limiting cases. Huang et al. 2000 [72, hereafter H00], modified the fireball hydrodynamics equations to account for a smooth evolution to the newtonian regime from the initial relativistic phase. We adopt their expressions to obtain the evolution of dynamical parameters of the expanding blastwave. Method of H00 is the following:
They modify the expression for $dE_{\rm th}$ as

$$dE_{\rm th} = d[(\Gamma - 1) m\, c^2] \tag{2.4}$$

Hence the amount of thermal energy remaining in the shock will be,

$$(1-\epsilon)\left[d\Gamma m + (\Gamma-1)dm\right]c^2$$

Using this expression with the condition of energy conservation

$$dE_{\rm kinetic} + dE_{\rm radiated} = 0$$

one obtains,

$$d\left[(\Gamma-1)(M_{\rm ej}+m)c^2 + (1-\epsilon)\Gamma E_{\rm th}\right] = -\epsilon\Gamma(\Gamma-1)dmc^2 \tag{2.5}$$

Solving the above expression gives the alternative to equation 2.1,

$$\frac{d\Gamma}{dm} = \frac{\Gamma^2-1}{M_{\rm ej}+\epsilon m + 2(1-\epsilon)\Gamma m} \tag{2.6}$$

Assuming $\epsilon = 0$, *ie.*,for the adiabatic evolution, this reduces to,

$$\frac{d\Gamma}{dm} = \frac{\Gamma^2-1}{M_{\rm ej}+2\Gamma m} \tag{2.7}$$

instead of equation 2.2.
The expression for dm is the same.

$$\frac{dm}{dr} = \Omega r^2 \rho(r) \tag{2.8}$$

dr/dt is given as,

$$\frac{dr}{dt} = (1+z)\beta c\Gamma(\Gamma+\sqrt{\Gamma^2-1}) \tag{2.9}$$

in lieu of equation 2.3. The solid angle Ω is defined as $2\pi(1-cos(\theta_j))$ where θ_j is the half opening angle of the shock at a distance r from the explosion. The half opening angle evolves with time as,

$$\frac{d\theta_j}{dr} = \frac{1}{\beta\Gamma}\left[\frac{c_s}{c}\right] \tag{2.10}$$

We obtain the dynamics of the fireball by numerical integration of equations (2.6), (2.8) and (2.9), for both spherical and conical geometry of the ejecta.

2.3.1 Calculation of velocity of sound in the shocked plasma

The jet opening angle varies according to the lateral expansion of the jet in its comoving frame. Velocity of this expansion is that of sound in the medium. In the ultra relativistic phase the sound velocity equals $(1/\sqrt{3})$ of that of the velocity of light. But once Γ and consequently the internal energy of the plasma decreases, the velocity of sound also drops. To calculate the sound velocity in the shocked medium we follow a different approach than that of Huang et al. The adiabatic sound velocity is defined as $c_s = dP/d\rho$ where P is the gas pressure and ρ is the mass density. Chandrasekhar 1989 [28] derives for the thermal energy density u of mono-atomic gas,

$$u = n\left[\frac{3K_3(\Theta) + K_1(\Theta)}{4K_2(\Theta)} - 1\right] m_1 c^2 \tag{2.11}$$

where n is the particle number density of the gas and m_1 is mass of a single particle. $\Theta = m_1 c^2/k_B T$, where T is the temperature of the gas. $K_j(\Theta)$ is the modified Bessel function of order j. In terms of temperature, thermal energy density is usually expressed as, $n\alpha(T)k_B T$, where $\alpha(T)$ parametrises the temperature dependence. It follows from the two expressions,

$$\alpha(T) = \Theta\left[\frac{3K_3(\Theta) + K_1(\Theta)}{4K_2(\Theta)} - 1\right] \tag{2.12}$$

In the non-relativistic regime $\alpha(T)$ approaches the familiar value 3/2 and in the relativistic limit it tends to 3. For a blast wave downstream plasma, with single particle rest mass m_1, the average thermal energy per particle $\alpha(T)k_B T$ can be written as $(\Gamma - 1)m_1 c^2$. ie.,

$$m_1 c^2\left[\frac{3K_3(\Theta) + K_1(\Theta)}{4K_2(\Theta)} - 1\right] = (\Gamma - 1)m_1 c^2 \tag{2.13}$$

from which we identify $(3K_3(\Theta) + K_1(\Theta))/4K_2(\Theta)$ with Γ. Temperature of the gas can be solved for in terms of Γ by inverting this relation. But the total energy density is independent of the dynamic regime of the gas and is given by, $u = \rho' c^2 = (u + n m_1 c^2)/V$ where ρ' is the total (rest mass + inertia) mass density. Using this expression we obtain,

$$\frac{\rho'}{P} = \Theta\frac{3K_3(\Theta) + K_1(\Theta)}{4K_2(\Theta)} = \Theta\Gamma \tag{2.14}$$

which gives sound velocity in the downstream in terms of Γ as,

$$\left[\frac{c_s}{c}\right]^2 = \frac{1}{\Theta\Gamma} \tag{2.15}$$

Let us examine the limiting values of the above expression and check the consistency. In the non-relativistic limit, $k_BT \ll m_1c^2$ ie., $\Theta \gg 1$, the Bessel function takes the form

$$K_j(\Theta) = \left[\frac{\pi}{2\Theta}\right]^{\frac{1}{2}} \exp(-\Theta)\left[1 + \frac{4n^2-1}{8\Theta}\right] \tag{2.16}$$

Substituting (equation 2.16) in (equation 2.15);

$$c_s^2 = \frac{k_BT}{m_1}\frac{4\left[1+\frac{15}{8\Theta}\right]}{3\left[1+\frac{35}{8\Theta}\right]+\left[1+\frac{3}{8\Theta}\right]} \tag{2.17}$$

Neglecting terms of the order of $1/\Theta$, expression for sound velocity in a non-relativistic gas is reduced to

$$c_s^2 = \frac{k_BT}{m_1} \tag{2.18}$$

Now, in the relativistic limit, ie., when $\Theta \ll 1$ The limiting expression for Bessel function is,

$$K_j(\Theta) = \frac{1}{2}\frac{(j-1)!}{(\frac{\Theta}{j})^j} \tag{2.19}$$

Substituting the above expression in (12), and neglecting terms $O(\Theta^2)$, we get for the sound velocity in a relativistic gas,

$$c_s^2 = \frac{k_BT}{m_1}\frac{8\Theta}{24} = \frac{c^2}{3} \tag{2.20}$$

2.3.2 Shell Thickness

We approximate the thickness of the post shock medium in its rest frame to be $dS' = c_s t_{co}$ [112], where

$$t_{co} = \int_0^r \frac{1}{\beta\Gamma^2} \tag{2.21}$$

We use primes to denote quantities measured in this frame. This shell thickness appears in the estimation of the optical depth of the swept up matter which in turn determines the synchrotron self absorption frequency of the plasma.

2.4 Magnetic Field

The magnetic energy density in the comoving frame of the plasma is considered as a fraction ϵ_B of the total thermal energy density u_{th} (See Piran 1999). We calculate u_{th} as $\frac{(\Gamma-1)mc^2}{V_{co}}$ where $V_{co} = \pi(r\theta_0 + c_s t_{co})^2 dS'$ (Ref: Rhoads 1999). θ_0 is the initial half opening angle of the jet. The comoving magnetic field density B can be obtained as

$$B = \left[8\epsilon_B \frac{(\Gamma-1)m}{(r\theta_j + c_s t_{co})^2 c_s t_{co}}\right]^{\frac{1}{2}} c \tag{2.22}$$

2.5 Electron energy distribution

As described in section 2.2, we assume the electrons to be distributed in a power-law of the form,

$$\begin{aligned} N(\gamma_e) &= K_e \gamma_e^{-p_1}, (\gamma_m \leq \gamma_e < \gamma_i) \\ &= K'_e \gamma_e^{-p_2} (\gamma_i \leq \gamma_e < \infty) \end{aligned} \tag{2.23}$$

where K_e is the normalisation constant. (see fig. 2.1)

K'_e can be written in terms of K_e as,

$$K'_e = K_e \gamma_i^{(p_2 - p_1)} \tag{2.24}$$

For an electron-proton plasma with upstream number density $n(r)$ at a distance r from the center of explosion, the post shock particle density and energy density are $4\Gamma n(r)$ and $4\Gamma(\Gamma-1)n(r)m_p c^2$ respectively (SPN98). Hence,

$$\int_{\gamma_m}^{\infty} N(\gamma_e) d\gamma_e = 4\Gamma n(r) \tag{2.25}$$

$$\int_{\gamma_m}^{\infty} \gamma_e m_e c^2 N(\gamma_e) d\gamma_e = \epsilon_e 4\Gamma(\Gamma-1)n(r)m_p c^2 \tag{2.26}$$

where ϵ_e is the fraction of thermal energy shared by the non-thermal electron population. m_p and m_e are the mass of the proton and the electron respectively. The

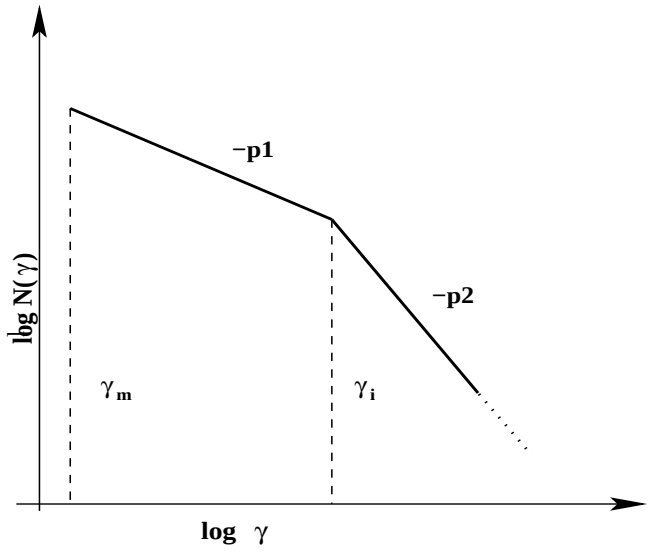

Figure 2.1. A schematic display of the modified electron distribution. Instead of the conventional single powerlaw, we assume a double power-law with slope $p_1(< 2)$ upto a lorentz factor γ_i and $p_2(> 2)$ above. p_2 could as well tend to ∞.

injection break γ_i in the electron spectrum is parametrised similar to B01 (equation 2.1), but since the treatment here extends to the non-relativistic evolution of the fireball too, we generalise this expression to be

$$\gamma_i = \xi(\beta\Gamma)^q \qquad 1 \leq \gamma_i \leq \infty \tag{2.27}$$

Solving equation 2.25 and equation 2.26 by assuming the distribution given by equation 2.23 and equation 2.27, one obtains the expressions for γ_m and K_e.

$$K_e = 4n(r)g_p \frac{m_p}{m_e} \frac{\epsilon_e}{\xi^{2-p_1}} \frac{1}{\beta^{q(2-p_1)}} \left[\Gamma - 1\right] \Gamma^{[1-q(2-p_1)]} \tag{2.28}$$

$$\gamma_m = \left[\frac{m_p}{m_e}\frac{\epsilon_e}{\xi^{2-p_1}} f_p\right]^{\frac{1}{(p_1-1)}} \left[\frac{1}{\beta^{q(2-p_1)}}\right]^{\frac{1}{(p_1-1)}} \left[\Gamma - 1\right]^{\frac{1}{p_1-1}} \Gamma^{-\frac{q(2-p_1)}{p_1-1}} \tag{2.29}$$

where $g_p = f_p(p_1 - 1)$ and $f_p = \frac{(2-p_1)(p_2-2)}{(p_1-1)(p_2-p_1)}$

2.6 New Spectral Break

Apart from the four spectral parameters described in section 1.8.7, the radiation spectrum emerging from a double slope electron distribution will exhibit an additional break which leads to a steeper slope at the "injection break" ν_i corresponding to the synchrotron frequency of an electron with Lorentz factor γ_i

$$\nu_i = \frac{0.286}{1+z}\frac{e}{\pi m_e c}\Gamma B \gamma_i^2 \tag{2.30}$$

2.7 Spectrum and Lightcurve

The afterglow radiation flux at any given time and frequency can be considered as a power law of the form $F_\nu(t) \propto \nu^\delta t^\alpha$. When any of the break frequencies described in section 1.8.7 is encountered, the value of δ changes and a different spectral segment starts.

Though in reality a smooth transition is expected from one spectral segment to the other, we joined the power-law segments with sharp breaks, except at ν_a. We incorporated absorption into the synchrotron optical depth, which along with the source function yields the flux at any given frequency.

The nature of the smooth transition at other breaks can be calculated by doing an integration over the emitting surface, taking care of light travel time effects. We have not attempted such an exercise in this thesis. We considered four possible regimes in the spectral evolution of the afterglow, depending upon the relative positions of the break frequencies. In the following subsections, we describe each spectral regime which is characterised by the positioning of the spectral breaks.

2.7.1 spectrum 1 ($\nu_a < \nu_m < \nu_i < \nu_c$)

The electrons are in a slow cooling regime (*ie.*, $\nu_m < \nu_c$). The spectral index in the range $\nu < \nu_a < \nu_m$ ($\delta = 2$), $\nu_a < \nu < \nu_m$ ($\delta = 1/3$) and $\nu_m < \nu < \nu_i$ ($\delta = -(p_1 - 1)/2$) are the same as in the standard model (see equation 1.29). The

spectral slope steepens at the injection break to $-(p_2-2)/2$ corresponding to the electron energy distribution index p_2. A further steepening to $-p_2/2$ happens at the cooling frequency.

2.7.2 spectrum 2 ($\nu_m < \nu_a < \nu_i < \nu_c$)

This case is similar to case 1 except the fireball is optically thick even above the synchrotron frequency. The peak flux which would have otherwise appeared at ν_m is suppressed by self absorption. As in the standard model, in the range $\nu < \nu_m < \nu_a$ $\delta = 2$ and between ν_a and ν_m, δ assumes the value 5/2. The spectral slope assumes value $-(p-1)/2$ for $\nu_a < \nu < \nu_i$, like the previous case. Above ν_i and ν_c, δ values are same as case-1.

2.7.3 spectrum 3 ($\nu_a < \nu_m < \nu_c < \nu_i$)

Here the cooling frequency falls below the injection break. The spectral shape is the same as that of the standard model till the injection break. At $\nu = \nu_i$, δ changes from $-p_1/2$ to $-p_2/2$.

2.7.4 spectrum 4 ($\nu_m < \nu_a < \nu_c < \nu_i$)

This is similar to the previous case, but the peak flux is suppressed by synchrotron self absorption. For $\nu < \nu_a$ the spectral slopes will change the same way as described in case 2.

Our code calculates the afterglow flux in any of these four regimes for spherical or collimated jet decelerating into an ambient medium of either homogeneous or stratified ($n(r) \propto r^{-s}$) density profile, and produces the lightcurve at the desired frequency. In figure 2.2 to 2.3 we display the spectral parameters ν_a, ν_m and ν_i (ν_c and f_m are not shown since their evolution is not affected by the modified electron energy spectrum) and lightcurves in radio (22 GHz), optical (4×10^{14} Hz) and x-ray (10^{18} Hz) bands for three different values of q. For the figures we considered a burst at $z = 1$, with spherical outflow of isotropic equivalent energy 10^{51} ergs and initial lorentz factor 350 in a homogeneous ambient medium of density 0.1

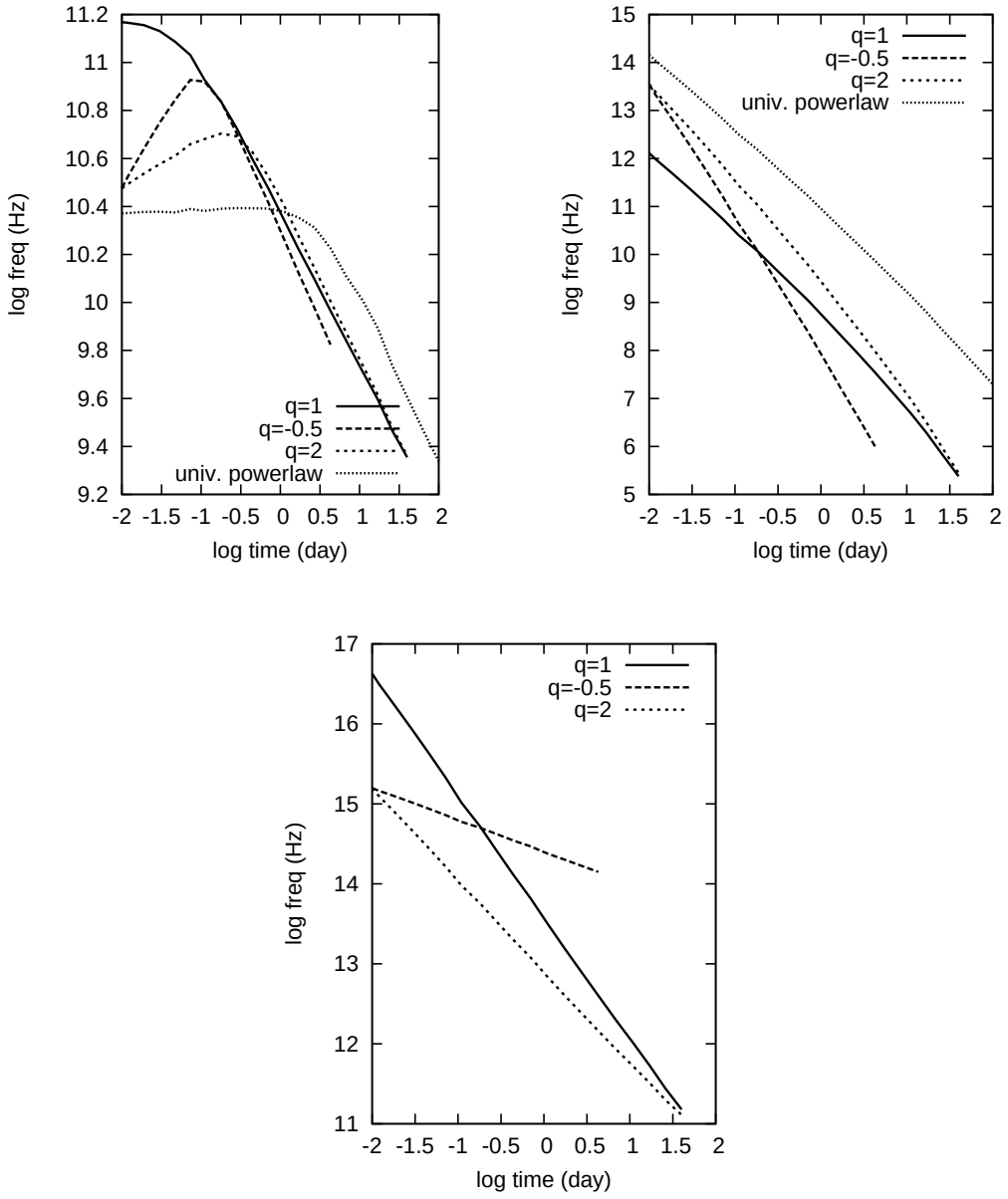

Figure 2.2. Spectral breaks ν_a (top left), ν_m (top right) and ν_i (bottom). All the figures are in logscale. For comparison, result of a 'single universal power law' with $p = 2.2$ is also shown (dash-dot curve). Since there is no ν_i for $p > 2$, we have not made a comparison with the standard model in this case. Notice that $q = 1$ and the single power law have the same temporal slope. Also see the change of evolution as q varies. The parameters gone into calculating the curves are listed at the end of section 2.7.

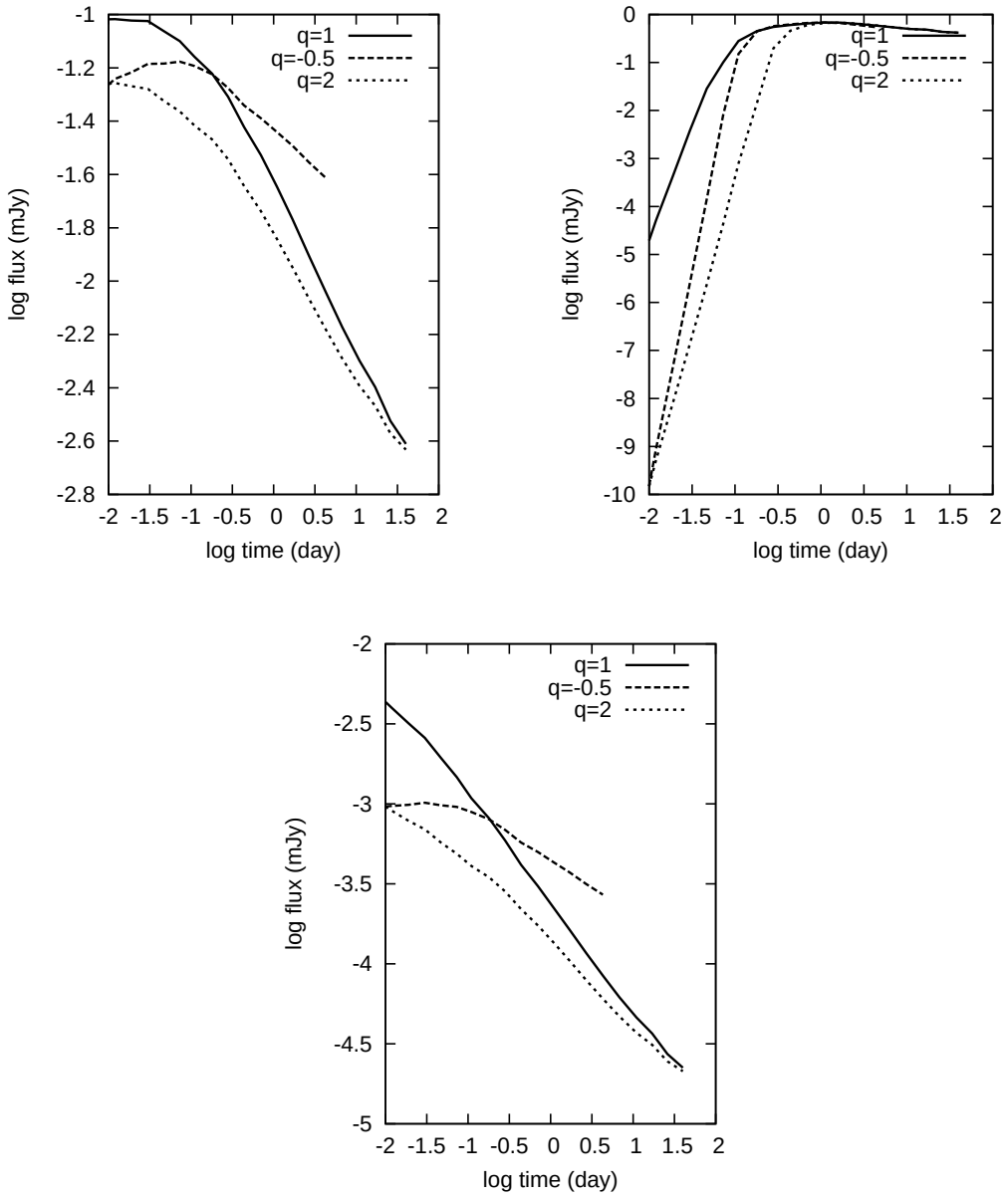

Figure 2.3. Optical lightcurve (4×10^{14} Hz), radio lightcurve (22 GHz) and x-ray lightcurve (10^{18} Hz) for the three different values of q.

atom/cc. The shock microphysics parameters are: $\epsilon_e = 0.1$, $\epsilon_B = 0.01$, $p_1 = 1.5$, $p_2 = 2.2$ and $\xi = 2000$.

2.8 Adiabatic Evolution in the Ultra-relativistic Limit

Modelling GRB afterglows till date have shown little evidence of a radiative evolution. We present analytical treatment for the evolution of an adiabatic blastwave ($\epsilon = 0$) in the ultra-relativistic regime($\Gamma \gg 1, \beta \sim 1$). In this case the equations for blastwave dynamics yield analytical solutions, and one will be able to derive the break frequencies also analytically. Hence it is possible to write down the temporal dependence of the flux in various spectral regimes explained in section 2.7. For the electron energy distribution given in section 2.5, table 2.1 lists the time dependences of spectral parameters, ν_m, ν_i, and ν_a. Time dependences of ν_c and f_{ν_m} will not be affected by the modification of electron energy spectrum. But we list these parameters also for completion. In Table 2.2 we list the final spectral and temporal indices ($\alpha\&\delta$) as functions of p_1, p_2 and q.

2.8.1 Dynamics

The three expressions which one has to solve here are,

$$\Gamma(r) = \sqrt{\Gamma_0 \frac{M_{\rm ej}}{m(r)}} \tag{2.31}$$

$$m(r) = \int_0^r \Omega(r')\, r'^2\, \rho(r')\, dr' \tag{2.32}$$

and

$$\frac{dt}{dr} = \frac{(1+z)}{2c}\frac{1}{\Gamma^2} \tag{2.33}$$

where, $\Omega(r) = \pi(\theta_0 + \frac{c_s}{c}\frac{1}{\Gamma(r)})^2$ and $\rho(r) \propto r^{-s}$. The index s is 0 for ISM and 2 for a density profile created by a constant velocity stellar wind. For the latter, a convenient normalisation, $\rho(r) = 5 \times 10^{-9} A_\star (r/10^{10})^{-2}$gm/cc [29] is used. All the solutions presented below are for pre-jet break evolution. For post jet-break dynamics, we will only present scaling laws (see table 2.1).
From equation (2.32), $m(r) = \pi\theta_0^2 \frac{\rho_0 r_0^3}{3-s}\left[\frac{r}{r_0}\right]^{3-s}$ hence,

$$\Gamma(r) = \sqrt{\frac{(3-s)E_0}{\Omega c^2}}(\rho_0 r_0^3)^{-1/2}\left[\frac{r}{r_0}\right]^{(s-3)/2} \tag{2.34}$$

$$r = \left[(4-s)(3-s)\frac{2c\,t}{1+z}\frac{E_0}{\Omega c^2}\frac{1}{\rho_0}\frac{1}{r_0^s}\right]^{\frac{1}{4-s}} \tag{2.35}$$

Expressions for $\Gamma(r)$, $r(t)$ and $\Gamma(t)$ for the two density profiles are :

$$\Gamma(r) = \begin{cases} 39.82 \left[\frac{\mathcal{E}_{\rm iso,52}}{n}\right]^{1/2} (r_{17})^{-3/2} & \text{(s=0)} \\ 1.33\times 10^4 \sqrt{\frac{\mathcal{E}_{\rm iso,52}}{A_\star}} \left[\frac{r}{10^{10}{\rm cm}}\right]^{-1/2} & \text{(s=2)} \end{cases} \tag{2.36}$$

$$r_{17} = \begin{cases} 4.25 \left[\frac{\mathcal{E}_{\rm iso,52}}{n}\frac{t_d}{1+z}\right]^{1/4} & \text{(s=0)} \\ 1.35\sqrt{\frac{\mathcal{E}_{\rm iso,52}}{A_\star}}\sqrt{\frac{t_d}{1+z}} & \text{(s=2)} \end{cases} \tag{2.37}$$

$$\Gamma(t) = \begin{cases} 4.14 \left[\frac{\mathcal{E}_{\rm iso,52}}{n}\right]^{1/8} \left[\frac{t_d}{1+z}\right]^{-3/8} & \text{s=0} \\ 3.62 \left[\frac{\mathcal{E}_{\rm iso,52}}{A_\star}\right]^{1/4} \left[\frac{t_d}{1+z}\right]^{-1/4} & \text{(s=2)} \end{cases} \tag{2.38}$$

where $\mathcal{E}_{\rm iso,52}$ is the isotropic equivalent energy normalised in units of 10^{52} ergs, and t_d is time t in days.

Following the assumption in section 2.4 and using $\Gamma \gg 1$, magnetic field B for the pre jet break evolution is,

$$B = \sqrt{8\pi\epsilon_B \frac{c_s}{c}\rho(r)}\,\Gamma\, c \tag{2.39}$$

And for $s = 0$ and $s = 2$, respectively,

$$B = \begin{cases} 0.88\,{\rm Gauss}\,\sqrt{\frac{c_s}{c}}\,\sqrt{\epsilon_B n}\,\left[\frac{\mathcal{E}_{\rm iso,52}}{n}\right]^{1/8}\left[\frac{t_d}{1+z}\right]^{-3/8} & \text{(s=0)} \\ 2.85\,{\rm Gauss}\,\sqrt{\frac{c_s}{c}}\,\mathcal{E}_{\rm iso,52}{}^{-1/4}\,\epsilon_B^{1/2}\,A_\star^{3/4}\,\left[\frac{t_d}{1+z}\right]^{-3/4} & \text{(s=2)} \end{cases} \tag{2.40}$$

2.8.2 Electron Energy Distribution

To calculate K_e and γ_m one can apply the limit of $\Gamma >> 1$ and $\beta = 1$ in equation 2.28 and equation 2.29 directly.

$$K_e = 4ng_p\frac{m_p}{m_e}\frac{\epsilon_e}{\xi^{2-p_1}}\Gamma^{2-q(2-p_1)} \tag{2.41}$$

$$\gamma_m = \left[\frac{m_p}{m_e}f_p\frac{\epsilon_e}{\xi^{2-p_1}}\right]^{1/(p_1-1)}\Gamma^{\frac{1-q(2-p_1)}{p_1-1}} \tag{2.42}$$

2.8.3 Spectral Parameters

The above expressions are used to obtain the spectral parameters for the ism ($s = 0$) and the wind ($s = 2$) density profiles. In this section, we are giving full expressions for both these cases.

$$f_m = \begin{cases} 210.45\,\mathrm{mJy}\ \phi_{p_1}\ \frac{1+z}{d^2_{L,\mathrm{Gpc}}} \sqrt{\frac{c_s}{c}}\ \sqrt{\epsilon_B\, n}\ \mathcal{E}_{\mathrm{iso},52} & (s=0) \\ 1021.5\mathrm{mJy}\ \frac{\phi_{p_1}(1+z)}{d^2_{L,\mathrm{Gpc}}} \sqrt{\mathcal{E}_{\mathrm{iso},52}\epsilon_B} A_\star \left[\frac{t_d}{(1+z)}\right]^{-1/2} & (s=2) \end{cases} \tag{2.43}$$

$$\nu_m = \begin{cases} 1.87\times10^7\mathrm{Hz}\ (17.14)^{\frac{1-q(2-p_1)}{p_1-1}}\ \left[\frac{m_p}{m_e}\, f_p\right]^{\frac{2}{p_1-1}}\ \sqrt{\frac{c_s}{c}}\ \frac{x_{p_1}}{1+z}\ \sqrt{\epsilon_B n}\ \epsilon_e^{\frac{2}{p_1-1}} \\ \xi^{-2\frac{2-p_1}{p_1-1}}\ \left[\frac{\mathcal{E}_{\mathrm{iso},52}}{n}\right]^{\frac{p_1+qp_1-2q}{4(p_1-1)}}\ \left[\frac{t_d}{(1+z)}\right]^{-\frac{3(p_1+qp_1-2q)}{4(p_1-1)}} & (s=0) \\ 5.77\times10^7\ \mathrm{Hz}\ (13.1)^y\ \sqrt{\frac{c_s}{c}}\ \frac{x_{p_1}}{1+z}\ \left[\frac{m_p}{m_e} f_{p_1}\right]^{\frac{2}{p_1-1}}\ \mathcal{E}_{\mathrm{iso},52}^{y/2}\ A_\star^{(1-y)/2} \\ \sqrt{\epsilon_B}\ \epsilon_e^{2/(p_1-1)}\ \xi^{\frac{-2}{(2-p_1)(p_1-1)}}\ \left[\frac{t_d}{(1+z)}\right]^{\frac{-(2+y)}{2}} & (s=2) \end{cases}$$

where $y = \frac{1-q(2-p_1)}{p_1-1}$

$$\nu_c = \begin{cases} 5.84\times10^{13}\ \mathrm{Hz}\ \left[\frac{c_s}{c}\right]^3\ \mathcal{E}_{\mathrm{iso},52}^{-1/2}\ n^{-1}\ \epsilon_B^{-3/2}\ [t_d(1+z)]^{-1/2} & (s=0) \\ 5.03\times10^{12}\,\mathrm{Hz}\ \frac{1}{(1+z)^3};\ \sqrt{\frac{c_s}{c}}\ \sqrt{\epsilon_B}\ A_\star^{-5/4}\ \mathcal{E}_{\mathrm{iso},52}^{1/4}\ \left[\frac{t_d}{(1+z)}\right]^{-1/4} & (s=2) \end{cases} \tag{2.44}$$

$$\nu_i \;=\; 1.3\times10^6\ \mathrm{Hz}\ \frac{(4.14)^{1+2q}}{1+z}\ \sqrt{\frac{c_s}{c}}\ \xi^2\ \sqrt{\epsilon_B\, n}\ \left[\frac{\mathcal{E}_{\mathrm{iso},52}}{n}\right]^{\frac{1}{4}(1+q)}\ \left[\frac{t_d}{(1+z)}\right]^{\frac{-3}{4}(1+q)} \tag{2.45}$$

$$\nu_a = \begin{cases} 3.66\times10^{16}\ \mathrm{Hz}\ (4.17)^{\frac{2(p_1+4+qp_1-2q)}{p_1+4}}\ (7346.58)^{\frac{2(2-2q+qp_1)}{p_1+4}}\ \left[0.2\sqrt{\frac{c}{c_s}}\right]^{\frac{p_1+2}{p_1+4}} \\ (2.61\times10^{19})^{\frac{p_1}{4+p_1}}\ (8.38\times10^{19})^{\frac{2}{4+p_1}}\ (8.2\times10^{-7})^{\frac{2(p_1-1)}{4+p_1}}\ (0.88)^{\frac{2+p_1}{4+p_1}}\ (3)^{\frac{p_1+1}{p_1+4}} \\ (4.14)^{\frac{2(2-2q+p_1q)}{4+p_1}}\ (0.64)^{\frac{2+p_1}{4+p_1}}\ \left[\sqrt{\frac{c}{c_s}}\right]^{\frac{p_1+2}{p_1+4}} \\ (2.3\times10^{-10})^{\frac{p_1}{p_1+4}}\left[\Gamma\left(\frac{3p_1+2}{12}\right)\ \Gamma\left(\frac{3p_1+22}{12}\right)\right]^{2/(p_1+4)}\ \left[1.87\times10^{-12}g_p\sqrt{3}\frac{c_s}{c}\right]^{\frac{2}{p_1+4}} \\ \mathcal{E}_{\rm iso,52}^{\frac{p_1+6+qp_1-2q}{4(p_1+4)}}\ \epsilon_B^{\frac{p_1+2}{2(p_1+4)}}\ \epsilon_e^{2/(p_1+4)}\ n^{\frac{p_1+6-qp_1+2q}{4(p_1+4)}}\ \xi^{-2\frac{2-p_1}{p_1+4}} \\ \left[\frac{t_d}{1+z}\right]^{\frac{-10-3p_1-3qp_1+6q}{4(p_1+4)}} \quad (s=0\quad \nu_a>\nu_m) \\ \\ 2.61\times10^{14}\ \mathrm{Hz}\ \ (4.14)^{\frac{10q+3p_1-5qp_1-8}{5(p_1-1)}}\ \left[\frac{c_s}{c}\right]^{23/40}\ \left[f_p\frac{m_p}{m_e}\right]^{-\frac{3p_1+2}{5(p_1-1)}} \\ \left[\frac{(4-p_1^2)(p_2-2)}{(p_1+2/3)(p_2-p_1)}\right]^{3/5}\ \epsilon_B^{1/5}\ \epsilon_e^{\frac{-1}{(p_1-1)}}\xi^{\frac{2-p_1}{p_1-1}}\ \mathcal{E}_{\rm iso,52}^{\frac{18-13p_1-10q+5p_1q}{40(p_1-1)}}\ n^{\frac{14-19p_1+10q-5p1q}{40(p_1-1)}} \\ \left[\frac{t_d}{1+z}\right]^{\frac{3(p_1-2)(q-1)}{8(p_1-1)}} \quad (s=0\quad \nu_a<\nu_m) \end{cases} \tag{2.46}$$

$$\nu_a = \begin{cases} (3.62)^{y_2}\ (3.42\times10^{53})^{\frac{1}{(p_1+4)}}\ (2.4\times10^{7})^{\frac{p_1}{(p_1+4)}}\ \left[g_p\frac{\epsilon_e}{\xi^{2-p_1}}\right]^{\frac{2}{(p_1+4)}} \\ \left[\sqrt{\frac{c_s}{c}}\sqrt{\epsilon_B}\right]^{\frac{p_1+2}{p_1+4}}\ \Gamma\left(\frac{3p_1+2}{12}\right)\ \Gamma\left(\frac{3p_1+22}{12}\right)\ \left[\frac{c_s}{c}\right]^{\frac{2}{p_1+4}} \\ \mathcal{E}_{\rm iso,52}^{\frac{qp_1-2q}{2(p_1+4)}}\ A_\star^{\frac{1.+2p_1+4q-2p_1q}{p_1+4}}\ \left[\frac{t_d}{(1+z)}\right]^{\frac{2q-2p_1-qp_1-8}{2(p_1+4)}} \quad (s=2\quad \nu_a>\nu_m) \\ 6.16\times10^{14}\ 3.62^{y_3}\ \left[\frac{p_1+2}{p_1+2/3}\right]^{3/2}\ \left[\frac{c_s}{c}\right]^{23/40}\ \left[\frac{m_p}{m_e}f_p\right]^{-\frac{2+3p_1}{5(p_1-1)}} \\ g_p^{3/5}\epsilon_B^{1/5}\ \mathcal{E}_{\rm iso,52}^{\frac{2}{5}+\frac{(p_1-2)(1-q)}{4(p_1-1)}}\ A_\star^{\frac{6}{5}-\frac{(p_1-2)(1-q)}{4(p_1-1)}}\ \left[\frac{\epsilon_e}{\xi^{2-p_1}}\right]^{\frac{3}{5}-\frac{2+3p_1}{5(p_1-1)}} \\ \left[\frac{t_d}{(1+z)}\right]^{\frac{7p_1-2-10q+5p_1q}{20(p_1-1)}} \quad (s=2\quad \nu_a>\nu_m) \end{cases}$$

where $y_2 = \frac{p_1+6-4q+2qp_1}{p_1+4}$ and $y_3 = \frac{(p_1-2)(1-q)}{p_1-1}$

2.8.4 Physical Parameters

Expressions for the five important physical parameters $\mathcal{E}_{\rm iso}$, $n(A_\star)$, ϵ_e, ϵ_B and ξ can be derived from that of the five spectral parameters, presented in section 2.8.3. Let us define C_f, C_m, C_c, C_i and C_a to be the combination of numerical and physical constants in the equations of f_{ν_m}, ν_m, ν_c, ν_i and ν_a respectively. From inverting the equations, one obtains,

We calculate the expressions for a constant ambient medium density profile.

$$\mathcal{E}_{\rm iso,52} = \left[\frac{\nu_m}{C_m}\right]^{\frac{2\Phi-4\varphi(\omega-\chi)}{\Phi}} \left[\frac{\nu_a}{C_a}\right]^{\frac{4\Phi-2\varphi(\omega-\chi)}{\Phi}} \left[\frac{\nu_c}{C_c}\right]^{\frac{2\Phi-2\varphi(\omega-3\chi)}{\Phi}} \tag{2.47}$$

$$n = \left[\frac{\nu_m}{C_m}\right]^{\frac{2(\omega-\chi)}{\Phi}} \left[\frac{\nu_a}{C_a}\right]^{\frac{\omega-\chi}{\Phi}} \left[\frac{\nu_c}{C_c}\right]^{\frac{\omega-3\chi}{\Phi}} \tag{2.48}$$

$$\epsilon_B = \left[\frac{f_{\nu_m}}{C_f}\right]^2 \left[\frac{\nu_m}{C_m}\right]^{\frac{2(\omega-\chi+2\Phi-4\omega\varphi-4\varphi\chi)}{\Phi}} \left[\frac{\nu_a}{C_a}\right]^{\frac{\omega-\chi+8\Phi-4\varphi\omega+4\varphi\chi}{\Phi}} \left[\frac{\nu_c}{C_c}\right]^{\frac{4(\Phi-\omega\varphi+\varphi\chi)}{\Phi}} \tag{2.49}$$

$$\xi = \left[\frac{\nu_i}{C_i}\right]^{1/2} \left[\frac{f_{\nu_m}}{C_f}\right]^{-1/2} \left[\frac{\nu_m}{C_m}\right]^{\frac{\omega-\chi\Phi-4\varphi\omega-\omega\chi}{2\Phi}} \left[\frac{\nu_c}{C_c}\right]^{\frac{\omega-\chi+8\Phi-4\varphi\omega+4\varphi\chi}{4\Phi}+\frac{(\omega-\chi)(q-1)}{8\Phi}-\frac{(2\Phi-\varphi\omega+\varphi\chi)(1+q)}{4\Phi}} \left[\frac{\nu_c}{C_c}\right]^{-\frac{\Phi-\omega\varphi+3\varphi\chi}{\Phi}+\frac{(q-1)(\omega-3\chi)}{4\Phi}-\frac{(1+q)(\Phi-\varphi\omega+3\varphi\chi)}{4\Phi}} \tag{2.50}$$

The expression for ϵ_e is complicated and we present it only in terms of the other parameters.

$$\epsilon_e = \left[\frac{\nu_a}{C_a}\right]^{1-p_1} [\mathcal{E}_{\rm iso,52}]^{(p1-1)a_1} [\epsilon_B]^{(p1-1)/5} [n]^{(p_1-1)a_1} [\xi]^{2-p_1} \tag{2.51}$$

where $\varphi = a_1 + m_1 - 1$

$\chi = 4a_2 + 2m_2 - 1$

$\psi = 4a_1 + 2m_1 - 3$

$\omega = 4a_2 + 2m_2 - 3$

$\Phi = 2\varphi\omega - \chi\psi$

$m_1 = \frac{p_1 - qp_1 - 2 + 2q}{8(p_1-1)}$

$m_2 = \frac{p_1 + qp_1 - 2q}{4(p_1-1)}$

$a_1 = \frac{14 - 19p_1 + 10q - 5p_1 q}{40(p_1-1)}$

$a_2 = \frac{18 - 13p_1 - 10q + 5p_1 q}{40(p_1-1)}$

Table 2.1. Temporal indices of the spectral parameters, for general q and s

frequency	before jet break	after jet break
ν_m	$\frac{s+(s-6)p_1-2q(2-p_1)(s-3)}{2(4-s)(p_1-1)}$	$\frac{2q-p_1-qp_1}{p_1-1}$
$\nu_a(<\nu_m)$	$\frac{s(10q-4-p_1-5p_1q)+15(-p_1+p_1q-2q+2)}{10(4-s)(p_1-1)}$	$-\frac{7p_1-5p_1q+10q-12}{10(p_1-1)}$
$\nu_a(>\nu_m)$	$\frac{s(2+p_1-4q+2p_1q)-6p_1-20+12q-6p_1q}{2(4-s)(p_1+4)}$	$\frac{(2q-4-p_1-qp_1)}{p_1+4}$
ν_i	$\frac{s(1+2q)-6(q+1)}{2(4-s)}$	$-(1+q)$
ν_c	$\frac{3s-4}{2(4-s)}$	0
f_{ν_m}	$-\frac{s}{2(4-s)}$	-1

2.9 Adiabatic Evolution in the Non-relativistic Limit

The dynamics of the fireball in this regime is the same as that of supernova remnants. The fireball by this time would have undergone a considerable lateral spread and the geometry can be approximated to be that of a spherical fireball. The solid angle Ω may now be set to 4π.

2.9.1 Dynamics

The radius will evolve with time according to,

$$\frac{dr}{dt} = \sqrt{\frac{3(\hat{\gamma}^2-1)E_0}{8\pi}}\,\frac{r^{-3/2}}{\rho(r)^{1/2}} \tag{2.52}$$

where E_0 is the total kinetic energy in the explosion, $\hat{\gamma}$ is the ratio of specific heats for the plasma (which can be approximated to 5/3 since one assumes the ambient medium to be mono-atomic and non-relativistic) Assuming $\rho(r)$ as $\rho_0\left[\frac{r}{r_0}\right]^{-s}$, and

Table 2.2. The spectral indices and lightcurve decay indices for various spectral regimes as a function of q. Note that α depends upon the value q assumes.

spectral segment	δ	α_1 (ISM,WIND)	α_2
$\nu < \nu_a < \nu_m < \nu_c$ $\nu < \nu_m < \nu_a < \nu_c$	2	$-\frac{(10-7p_1+3p_1q-6q)}{8(p_1-1)}, \frac{6-5p_1+p_1q-2q}{4(1-p_1)}$	$\frac{3p_1-6-3p_1q+6q}{6(p_1-1)}$
$\nu_a < \nu < \nu_m < \nu_c$	$\frac{1}{3}$	$\frac{p_1+p_1q-2q}{4(P_1-1)}, \frac{2-p_1+p_1q-2q}{6(P_1-1)}$	$\frac{-2p_1+3-2+p_1}{3(p_1-1)}$
$\nu_m < \nu < \nu_a$	$\frac{5}{2}$	$\frac{5}{4}, \frac{7}{4}$	1
$\nu_m < \nu < \nu_i < \nu_c$ $\nu_m < \nu < \nu_c < \nu_i$	$-\frac{(p_1-1)}{2}$	$-\frac{3}{8}(p_1+p_1q-2q), \frac{(2q-p_1q-2p_1-1)}{4}$	$\frac{p_1(1+q)+2(q-1)}{2}$
$\nu_m < \nu_i < \nu < \nu_c$	$-\frac{(p_2-1)}{2}$	$\frac{3}{8}(2q-p_2q-p_2), \frac{1}{4}(2q-p_2(2+q)-1)$	$\frac{2(q-1)-p_2(1+q)}{2}$
$\nu_m < \nu_c < \nu < \nu_i$	$-\frac{p_1}{2}$	$\frac{1}{8}(2(3q-1)-3p_1(1+q)), \frac{1}{4}(2q-p_1q-2p_1)$	$\frac{2(q-1)-p_1(q+1)}{2}$
$\nu_m < \nu_i < \nu_c < \nu$ $\nu_m < \nu_c < \nu_i < \nu$	$-\frac{p_2}{2}$	$\frac{1}{8}(3(q-p_2-p_2q)-2), \frac{1}{4}(2q-2p_2-p_2q)$	$\frac{2(q-1)-p_2(q+1)}{2}$

solving the above equation, one obtains,

$$r = \left[\frac{(5-s)^2 E_0 r_0^{-s}}{6\pi\rho_0}\right]^{1/(5-s)} t^{2/(5-s)} \tag{2.53}$$

and

$$\beta = \frac{2}{(5-s)c}\left[\frac{(5-s)^2 E_0 r_0^{-s}}{6\pi\rho_0}\right]^{1/(5-s)} t^{\frac{s-3}{5-s}} \tag{2.54}$$

For $s = 0$,

$$r = 2.51 \times 10^{15}\,\mathrm{cm}\,(\mathcal{E}_{52}/\mathrm{n})^{1/5}\,\left[\frac{\mathrm{t}}{\mathrm{t_{NR}}}\right]^{2/5}\,\left[\frac{\mathrm{t_{NR}}}{1+\mathrm{z}}\right]^{2/5}$$

$$\beta = 3.34 \times 10^{4}\,(\mathcal{E}_{52}/n)^{1/5}\,\left[\frac{t}{t_{\mathrm{NR}}}\right]^{-3/5}\,\left[\frac{t_{\mathrm{NR}}}{1+z}\right]^{-3/5}$$

For $s = 2$,

$$r = 4.93 \times 10^{13}\mathrm{cm}\,(\mathcal{E}_{52}/\mathrm{A}_\star)^{1/3}\,\left[\frac{\mathrm{t}}{\mathrm{t_{NR}}}\right]^{2/3}\,\left[\frac{\mathrm{t_{NR}}}{1+\mathrm{z}}\right]^{2/3}$$

$$\beta = 1094.75\,(\mathcal{E}_{52}/A_\star)^{1/3}\,\left[\frac{t}{t_{\mathrm{NR}}}\right]^{-1/3}\,\left[\frac{t_{\mathrm{NR}}}{1+z}\right]^{-1/3}$$

where t_{NR} is the reference time for non-relativistic transition, which can be set to the time when $\Gamma \to 1$.

2.9.2 Electron energy spectrum

The thermal energy density in the shock downstream is

$$u_{\mathrm{th}} = \frac{9c^2\rho_0}{8}\,\beta^2\,(r/r_0)^{-s} \tag{2.55}$$

The expressions for electron number and energy will give, respectively,

$$\frac{K_e}{(p_1-1)\gamma_m^{p_1-1}} = 4\rho_0/m_p\,(r/r_0)^{-s} \tag{2.56}$$

$$\frac{K_e m_e}{g_p}\,\gamma_i^{(2-p_1)} = \frac{9c^2\rho_0}{2}\epsilon_e\,\beta^2\,(r/r_0)^{-s} \tag{2.57}$$

after assuming $\hat{\gamma}$ to be 5/3. Solving equation 2.57 and equation 2.56, one obtains the expressions for K_e and γ_m.

$$K_e = \frac{9}{2}g_p\frac{\rho_0}{m_e}\,\frac{\epsilon_e}{\xi^{2-p_1}}\,(r/r_0)^{-s}\,\beta^{2-q(2-p_1)} \tag{2.58}$$

$$\gamma_m = \left[\frac{9}{8}f_p\frac{m_p}{m_e}\frac{\epsilon_e}{\xi^{2-p_1}}\right]^{1/(p_1-1)}\,\beta^{\frac{2-q(2-p_1)}{p_1-1}} \tag{2.59}$$

2.9.3 Spectral Parameters

The magnetic field energy density is assumed, as usual, to be a fraction ϵ_B times the thermal energy density. ie.,

$$B = \sqrt{9\pi\epsilon_B\beta^2 c^2 \rho(r)} \tag{2.60}$$

which for $s = 0$ will reduce to,

$$4.72 \times 10^{-6}\mathrm{Gauss}\ \sqrt{\epsilon_\mathrm{B}\,\mathrm{n}}\ (\mathcal{E}_{52}/\mathrm{n})^{1/5}\ \left[\frac{\mathrm{t}}{\mathrm{t_{NR}}}\right]^{3/5}\ \left[\frac{\mathrm{t_{NR}}}{1+\mathrm{z}}\right]^{3/5}$$

and for $s = 2$,

$$2.51 \times 10^{6}\mathrm{Gauss}\ \sqrt{\epsilon_\mathrm{B}\,\mathrm{A}_\star}\left[\frac{\mathrm{t}}{\mathrm{t_{NR}}}\right]^{-1}\ \left[\frac{\mathrm{t_{NR}}}{1+\mathrm{z}}\right]^{-1}$$

Having obtained all the ingredients for the spectral parameters, we proceed to calculate them now. Here we calculate the four spectral breaks, ν_a, ν_m, ν_c and ν_i and the peak flux f_m. All the parameters are in cgs units.

$$f_m = \frac{2.94 \times 10^{-21}}{d_L^2\, a}\ 0.053^{(p_1-1)}\ \Gamma\!\left(\tfrac{3p_1+2}{12}\right)\ \Gamma\!\left(\tfrac{3p_1+22}{12}\right)\ r^3 \frac{K_e\ B}{\gamma_m^{p_1-1}} \tag{2.61}$$

$$\nu_m = 2.8 \times 10^{6}\ \frac{x_p}{(1+z)}\ B\ \left[2065.7 f_p \frac{\epsilon_e}{\xi^{(2-p_1)}}\right]^{2/(p_1-1)}\ \beta^{\frac{2[2-q(2-p_1)]}{(p_1-1)}} \tag{2.62}$$

$$\nu_c = 4.81 \times 10^{23}\ \frac{1}{B^2}\left[\frac{t}{t_{\mathrm{NR}}}\right]^{-2}\ \left[\frac{t_{\mathrm{NR}}}{1+z}\right]^{-2} \tag{2.63}$$

$$\nu_i = 8.0 \times 10^{5}\ \frac{1}{(1+z)}\ B\xi^2\beta^{2q} \tag{2.64}$$

$$\nu_a = \begin{cases} 4.72\left[\frac{p_1+2}{p_1+2/3}\ K_e\right]^{3/5}\ \gamma_m^{-(3p_1+2)/5}\ r^{3/5}B^{2/5} & (\text{for } \nu_a > \nu_m) \\ (6.72\times10^{-13})^{\frac{p_1-1}{p_1+4}}\ (1.25\times10^{19})^{\frac{p_1}{p_1+4}}\ (7\times10^{-5})^{\frac{1}{p_1+4}} & \\ \left[\Gamma\!\left(\frac{3p_1+2}{12}\right)\ \Gamma\!\left(\frac{3p_1+22}{12}\right)\right]^{\frac{2}{p_1+4}}\ B^{\frac{p_1+2}{p_1+4}}\ \frac{rK_e}{a}^{\frac{2}{p_1+4}} & (\text{for } \nu_a < \nu_m) \end{cases} \tag{2.65}$$

The factor a in equation 2.61 takes care of the dependence the shell thickness has on the radius r, it is of the order of 10.

2.10 Synchrotron Self Compton (SSC)

The contribution to the total flux from synchrotron photons which are compton scattered due to the non-thermal electron spectrum itself, can be significant towards higher energies.

We calculated the compton component following the method adopted by Sari & Esin [117]. Initially we estimated the approximate ratio of Inverse Compton (IC) to synchrotron luminosities. (The calculations are done only for a constant ambient density profile and a slow cooling regime)

The spectral parameters for the IC spectrum are assumed following Sari & Esin [117].

$$\nu_m^{\rm IC} = 2\gamma_m^2 \nu_m^{\rm syn} \tag{2.66}$$
$$\nu_c^{\rm IC} = 2\gamma_c^2 \nu_c^{\rm syn} \tag{2.67}$$
$$\nu_i^{\rm IC} = 2\gamma_i^2 \nu_i^{\rm syn} \tag{2.68}$$
$$\nu_a^{\rm IC} = 2\gamma_m^2 \nu_a^{\rm syn} \tag{2.69}$$
$$f_{\nu_m}^{\rm IC} = f_{\nu_m}^{\rm syn} \sigma_T \, n \, r \tag{2.70}$$

For $\nu_m^{\rm syn} \leq \nu_i^{\rm syn} \leq \nu_c^{\rm syn}$, energy emitted by compton process peaks at $\nu_c^{\rm IC}$ and that by synchrotron process will peak at $\nu_c^{\rm syn}$. Hence, $x = L^{\rm IC}/L^{\rm syn}$, can be calculated as,

$$\begin{aligned} x &\approx \frac{\nu_c^{\rm IC} \; f_{\nu_c}^{\rm IC}}{\nu_c^{\rm syn} \; f_{\nu_c}^{\rm syn}} \\ &\approx 700 \mathcal{R}_{-7} \; \gamma_{c,7}^2 \left[\frac{\gamma_{m,500}}{\gamma_{i,5}}\right]^{(p_1-1)_{0.5}} \left[\frac{\gamma_{i,5}}{\gamma_{c,7}}\right]^{(p_2-1)_{1.5}} \end{aligned} \tag{2.71}$$

The energy peaks at ν_i for both the processes, if $\nu_m^{\rm syn} \leq \nu_c^{\rm syn} \leq \nu_i^{\rm syn}$

$$\begin{aligned} x &\approx \frac{\nu_i^{\rm IC} \; f_{\nu_i}^{\rm IC}}{\nu_i^{\rm syn} \; f_{\nu_i}^{\rm syn}} \\ &\approx 700 \mathcal{R}_{-7} \; \gamma_{i,7} \; \gamma_{c,5} \left[\frac{\gamma_{m,500}}{\gamma_{i,7}}\right]^{(p_1-1)_{0.5}} \end{aligned} \tag{2.72}$$

where $\gamma_{e,n} = \gamma_e/10^n$, $\gamma_{m,500} = \gamma_m/500$, $\mathcal{R}_{-7} = \frac{f^{\rm IC}_{\nu_m}/f^{\rm syn}_{\nu_m}}{10^{-7}}$ and $(p-1)_f = (p-1)/f$.

In both the cases, the energy peaks at very high frequencies (for both the cases, the peak will be $\sim 10^{21}$ Hz $\frac{B}{0.1\rm G}\frac{\Gamma}{100}$). In currently observable frequencies, the contribution from SSC for hard electron distribution could be insignificant.

However, to obtain the complete SSC spectrum we estimated the IC flux from full numerical integration over the photon and electron spectra.

We used the expression given by Sari & Esin 2001 [117] for the inverse compton flux due to an electron energy spectrum $N(\gamma)$ of the form given by equation 1.11 and the synchrotron radiation spectrum $f^{\rm syn}_\nu$ generated by this electron energy spectrum,

$$f^{\rm IC}_\nu = r\sigma_T \int_{\gamma_m}^{\infty} d\gamma\, N(\gamma) \int_0^{x_0} dx f^{\rm syn}_\nu(x) \tag{2.73}$$

where $x_0 \sim 0.5$

The synchrotron and compton fluxes obtained by the above calculation is displayed in figure 2.4

2.11 Physical Implications

Having calculated the spectral evolution for the double power law with a general value of q, a discussion on the physical origin of such distributions and expected values of the parameter are due.

2.11.1 $q = 1$: The minimum energy for electron acceleration

Origin of non-thermal electron distribution in the fireball plasma is usually attributed to Diffusive Shock Acceleration (DSA), which is a variant of the first order fermi mechanism [41]. An already relativistic particle diffuses through the medium on either side of the shock by scattering on magnetic irregularities, and gain energy on each scatter [9, 19]. A major difficulty in accelerating electrons by this mechanism, is the need of an 'injection process' for the sub and mildly

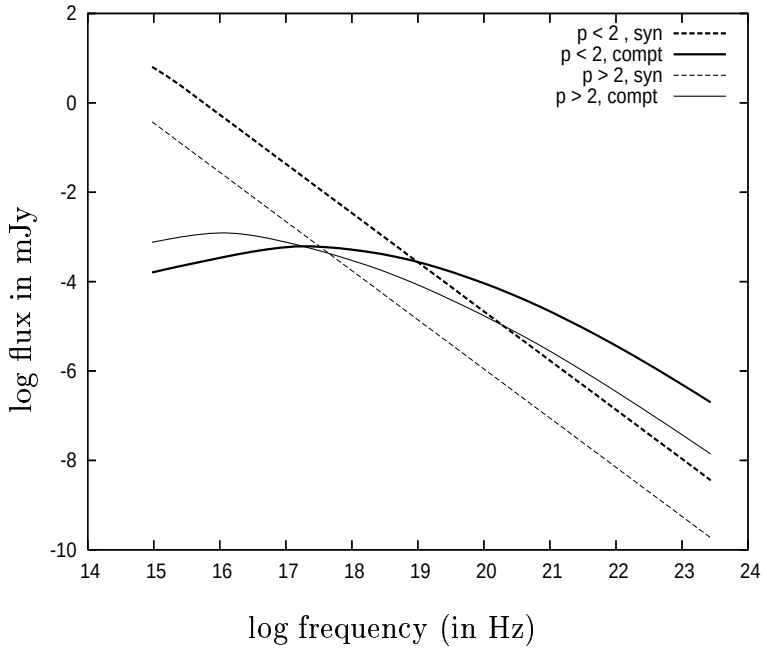

Figure 2.4. The compton contribution from hard electron energy spectrum, in comparison with that from a steep spectrum. For frequencies less than 10^{19} Hz, the contribution from SSA is rather low for $p < 2$ spectrum. The parameters used for calculation are, $\mathcal{E}_{\rm iso,52} = 10^2$, $n = 100$, $\epsilon_e = 0.3$ and $\epsilon_B = 10^{-3}$. For hard spectrum $p_1 = 1.8$, $p_2 = 2.2$, $q = 1$ and $\xi = 5000$ are used, and for steep spectrum a p of 2.2 is used. The displayed spectra are for ~ 5 days.

relativistic electrons. Those electrons with energy lower than that of the thermal protons will not perceive the shock as a discontinuity [84]. Hence DSA has a threshold lorentz factor ($\gamma_{\rm acc}$) for electrons, which equals to $m_p\Gamma/m_e$. Below $\gamma_{\rm acc}$, the acceleration process is unable to operate. The assumption made in the external shock model of GRB afterglow is that a fraction ϵ_e of the thermal energy produced by the shock in the downstream plasma goes into the electron population which extends from a lorentz factor γ_m to ∞. As is obvious from figure 2.5, for a low ϵ_e the γ_m estimated by the standard afterglow model works out to be much lower than γ_{acc}. This clearly says that the 'universal spectrum' can not be applied for $\gamma_m \leq \gamma_e < \gamma_{\rm acc}$. We conjecture an unknown pre-acceleration mechanism to operate in this range, to produce a flat spectral index for electron distribution in that range. (A candidate process could be the 'cyclotron resonance

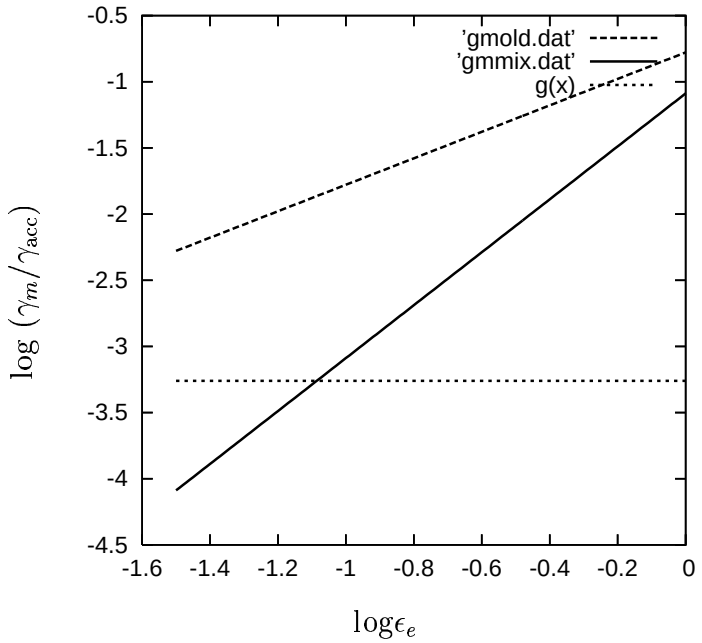

Figure 2.5. γ_m from the universal powerlaw and the double slope spectrum in a comparison. x-axis is ϵ_e and y-axis is γ_m normalised by $\gamma_{\rm acc}(=\frac{m_p\Gamma}{m_e})$. The universal powerlaw is for $p = 2.2$, and γ_m computed using that equals to $\gamma_{\rm acc}$ only when $\epsilon_e = 1$, which is not an achievable condition. This implies that the universal powerlaw cannot be extended down to the values of electron lorentz factors which it conventionally includes. It must stop around $\gamma_{\rm acc}$. The double slope spectrum is calculated for $p_1 = 1.5$ and $p_2 = 2.2$, and for the whole range of ϵ_e, γ_m remains below the injection threshold as expected from the pre-acceleration mechanism

mechanism' proposed for explaining the multi-band spectrum of crab nebula [71]) In this situation the lower cutoff of the universal spectrum, $\gamma_{\rm acc}$, may be identified with the injection break γ_i. As

$$\gamma_i = \frac{m_p}{m_e}\Gamma \tag{2.74}$$

the value of q in this picture works out to be 1.

When $q = 1$, the dependence of γ_m and K_e on Γ will be reduced to that of $p > 2$ case. γ_i and γ_m will be similar functions of time. Thus the frequencies ν_m and ν_a will follow the same time evolution as they do in case of the standard model. Since time dependences of ν_c and f_m are not affected by the change in the electron energy spectrum, this brings the lightcurve evolution to be similar to

that of the standard case (See figure 2.2). Table 2.3 summarizes temporal slopes of various spectral regimes in this case.

Table 2.3. The spectral indices (δ) and lightcurve decay indices (α) for various spectral regimes if $q = 1$. The usual $p > 2$ expressions are recovered.

spectral segment	δ	α_1 (ISM,WIND)	α_2
$\nu < \nu_a < \nu_m < \nu_c$ $\nu < \nu_m < \nu_a < \nu_c$	2	$\frac{1}{2}, 1$	0
$\nu_a < \nu < \nu_m < \nu_c$	$\frac{1}{3}$	$\frac{1}{2}, 0$	$-\frac{1}{3}$
$\nu_m < \nu < \nu_a$	$\frac{5}{2}$	$\frac{5}{4}, 1$	1
$\nu_m < \nu < \nu_i < \nu_c$ $\nu_m < \nu < \nu_c < \nu_i$	$-\frac{(p_1-1)}{2}$	$\frac{-3}{4}(p_1-1), -\frac{1}{4}(3p_1-1)$	$-p_1$
$\nu_m < \nu_i < \nu < \nu_c$	$-\frac{p_2-1}{2}$	$-\frac{3}{4}(p_2-1), -\frac{1}{4}(3p_2-1)$	$-p_2$
$\nu_m < \nu_c < \nu < \nu_i$	$-\frac{p_1}{2}$	$-\frac{1}{4}(3p_1-2), -\frac{1}{4}(3p_1-2)$	$-p_1$
$\nu_m < \nu_i < \nu_c < \nu$ $\nu_m < \nu_c < \nu_i < \nu$	$-\frac{p_2}{2}$	$-\frac{1}{4}(3p_2-2), -\frac{1}{4}(3p_2-2)$	$-p_2$

2.11.2 $q = -0.5$: The maximum threshold of particle acceleration

A double slope spectrum can also originate due to the upper cutoff of the particle acceleration process. The acceleration process becomes ineffective when the acceleration timescale exceeds the timescale for radiative energy loss [1].

The maximum electron lorentz factor from this process can be calculated by equating the downstream residence time t_d with the synchrotron cooling time $t_{\rm syn}$

[2, 37], which yields, $\gamma_u = \sqrt{3e/(B\sigma_T)}$ (This result is same as DC01). Substituting the expression for B, one obtains $q = -0.5$ and $\xi \sim 10^7$. Above this upper cutoff, which will be identified as γ_i, the energy spectrum will fall off quickly giving rise to a large value of p_2.

If this process is responsible for the double slope spectrum, one would need the Fermi process to produce a $p < 2$ electron spectrum, which is contrary to the results of numerical simulations, where a $p \sim 2.2$ power law is usually obtained. Nevertheless, a wide range of p values are observed, including hard spectra, in situations involving relativistic shocks [122].

2.12 Conclusion

Almost all of theoretical and modelling work in GRB afterglow physics, by default, assume a single steep power law for the distribution of electrons in the downstream plasma. This assumption is motivated by the result of numerical simulations involving relativistic shock acceleration where a universal $p \sim 2.2$ is often obtained and also by the observational evidence of a majority of $p > 2$ afterglows.

The presence of $p < 2$ spectrum, in a minority of cases, has however not received a fair share of attention. Calculations to derive the physical parameters of the burst in such cases are often not done consistently. Early attempts (DC01 & PK01), to model GRB afterglows with hard electron energy spectrum had several loop holes. DC01 does the calculation only for the special case which is described in section 2.11.2. In PK01, the evolution of ν_i and its significance in determining the spectral evolution has been ignored.

We have, instead taken the approach of parametrising the temporal evolution of γ_i (and thereby leaving room to account for different possible physical processes that could determine γ_i) as $\gamma_i \propto \Gamma^q$ and obtaining the afterglow flux decay index for different values of q. We have obtained expressions to calculate the observables from the physical parameters of the system which in turn can be used to derive the latter.

The upper cut-off of the electron energy spectrum can have its origin in more than one physical mechanisms. In section 2.2, we have listed a couple of them

which are known within the current understanding of the physics of relativistic shocks as sites of particle acceleration. The numerical simulations which are done at present, give rise to a more or less 'universal' value of p, which is not supported by observations. A more detailed study of relativistic shock acceleration could perhaps solve this mystery.